Chinese Chemical Letters 36 (2025) 110140

Contents lists available at ScienceDirect

Chinese Chemical Letters

journal homepage: www.elsevier.com/locate/cclet

Tetrahedral framework nucleic acids prevent epithelial-mesenchymal transition-mediated diabetic fibrosis by targeting the Wnt/β-catenin signaling pathway

Yujie Zhu[a,b], Ruijianghan Shi[a,b], Weitong Lu[a,b], Yang Chen[c], Yunfeng Lin[a,b], Sirong Shi[a,b,*]

[a] State Key Laboratory of Oral Diseases & National Center for Stomatology & National Clinical Research Center for Oral Diseases, West China Hospital of Stomatology, Sichuan University, Chengdu 610041, China
[b] Sichuan Provincial Engineering Research Center of Oral Biomaterials, Chengdu 610041, China
[c] Department of Pediatric Surgery, Department of Liver Surgery & Liver Transplantation Center, West China Hospital of Sichuan University, Chengdu 610041, China

ARTICLE INFO

Article history:
Received 3 April 2024
Revised 16 June 2024
Accepted 18 June 2024
Available online 19 June 2024

Keywords:
Tetrahedral framework nucleic acids
DNA nanomaterials
Diabetic kidney disease
Renal fibrosis
Antifibrotic therapy

ABSTRACT

Diabetic kidney disease (DKD) is recognized as a severe complication in the development of diabetes mellitus (DM), posing a significant burden for global health. Major characteristics of DKD kidneys include tubulointerstitial oxidative stress, inflammation, excessive extracellular matrix deposition, and progressing renal fibrosis. However, current treatment options are limited and cannot offer enough efficacy, thus urgently requiring novel therapeutic approaches. Tetrahedral framework nucleic acids (tFNAs) are a novel type of self-assembled DNA nanomaterial with excellent structural stability, biocompatibility, tailorable functionality, and regulatory effects on cellular behaviors. In this study, we established an *in vitro* high glucose (HG)-induced human renal tubular epithelial cells (HK-2 cells) pro-fibrogenic model and explored the antioxidative, anti-inflammatory, and antifibrotic capacity of tFNAs and the potential molecular mechanisms. tFNAs not only effectively alleviated oxidative stress through reactive oxygen species (ROS)-scavenging and activating the serine and threonine kinase (Akt)/nuclear factor erythroid 2-related factor 2 (Nrf2)/heme oxygenase-1 (HO-1) signaling pathway but also inhibited the production of pro-inflammatory factors such as tumor necrosis factor (TNF-α), interleukin-1β (IL-1β), and interleukin-6 (IL-6) in diabetic HK-2 cells. Additionally, tFNAs significantly downregulated the expression of Collagen I and α-smooth muscle actin (α-SMA), two representative biomarkers of pro-fibrogenic myofibroblasts in the renal tubular epithelial-mesenchymal transition (EMT). Furthermore, we found that tFNAs exerted this function by inhibiting the Wnt/β-catenin signaling pathway, preventing the occurrence of EMT and fibrosis. The findings of this study demonstrated that tFNAs are naturally endowed with great potential to prevent fibrosis progress in DKD kidneys and can be further combined with emerging pharmacotherapies, providing a secure and efficient drug delivery strategy for future DKD therapy.

Diabetic kidney disease (DKD) is a severe complication in diabetes mellitus (DM) and is acknowledged as the leading cause of end-stage renal disease (ESRD) [1]. Major histopathological changes in DKD kidneys involve both glomerulus and tubule interstitium, characterized by basement membrane thickness, extracellular matrix expansion, and fibrosis [2,3]. Uncontrolled renal fibrosis will further develop into irreversible renal sclerosis and ultimately renal failure, which suffers from poor treatment options (dialysis or kidney transplantation) and increased mortality risk [3]. Nowadays, due to the development of the economy and alteration of lifestyle, the incidence of obesity and ensuing type 2 diabetes in developing countries is continuously growing. It is predicted that by 2035, the global population of diabetes mellitus patients will surpass 600 million, significantly increasing the public burden [4]. Therefore, effective preventative and therapeutic strategies are urgently needed to cope with this serious issue.

Focusing on the histopathological process of DKD, accumulating evidence suggests that tubulointerstitial inflammation, especially in proximal tubular epithelial cells, plays a pivotal role in renal fibrosis [5]. On the one hand, hyperglycemia can induce hyper-reabsorption of glucose in proximal tubular epithelial cells, significantly increasing mitochondria activities and excessive reactive oxygen species (ROS) production, resulting in oxidative stress.

* Corresponding author.
E-mail address: sirongshi@scu.edu.cn (S. Shi).

https://doi.org/10.1016/j.cclet.2024.110140
1001-8417/

Then high concentrations of intracellular ROS can act as a potent pro-inflammatory factor to upregulate the expression of tumor necrosis factor-α (TNF-α), interleukin-1β (IL-1β), and IL-6, further contributing to tubulointerstitial inflammation and ensuing fibrosis. On the other hand, many studies also support that high glucose (HG) will activate the Wnt signal transduction pathway, causing epithelial-mesenchymal transition (EMT) [2]. In DKD, nearly 30% of fibroblasts or myofibroblasts originate from tubular epithelial cells, exerting a dominant role in extracellular matrix production and secretion [3,6]. Although pharmacotherapies *via* renin-angiotensin-aldosterone system (RAAS) blockers and sodium-glucose co-transporter 2 (SGLT2) inhibitors have been demonstrated to alleviate the progression of renal fibrosis, the collateral outcomes remain unsatisfactory, requiring other alternative solutions [7].

With the rapid development of nanotechnology, various nanostructures with excellent physical, chemical, and biological properties consecutively emerged, providing innovative biological detection, diagnosis, and treatment strategies to address current clinical challenges [8-10]. Among these new-generation nanomaterials, tetrahedral framework nucleic acids (tFNAs), a novel three-dimensional DNA nanomaterial initially proposed by Turberfield in 2004 [11], came out due to their prominent performance. Based on the Waston-Crick base-pairing principle, the synthesis of tFNAs is convenient and efficient meanwhile. The "one-pot" synthesis protocol enables four precisely designed isometric single-stranded DNA (ssDNA) self-assemble into stable tetrahedrons, with up to 90% high yields [12,13], laying a solid foundation for further construction of functional tFNAs complex [14-17]. In addition, tFNAs also possess excellent biocompatibility, cellular endocytosis, tailorable functionality, and particularly innate regulatory effects on cell behavior [18]. For example, abundant evidence has demonstrated that tFNAs can effectively scavenge excessive ROS and regulate relevant signaling pathways through multi-facet mechanisms, protecting cells from oxidative stress and inflammatory damage [19-22]. Moreover, the antifibrotic advantages of tFNAs and derived functional complexes have also been widely verified in previous studies, including scarless skin wound healing [23-25], attenuated liver cirrhosis [26,27], as well as acute kidney injury (AKI) [28]. However, to the best of our knowledge, few reports have evaluated the antifibrotic effects of simple tFNAs on the DKD HG microenvironment. Given the aforementioned DKD pathological origin and tFNAs biochemical basis, we assumed that tFNAs could also exert protective impacts on diabetic renal tubular epithelial cells. According to the study of Zhang *et al.* and Lu *et al.*, 30 mmol/L glucose (HG) can induce adequate diabetic injury in human renal tubular epithelial cells (HK-2) [29-31]. Therefore, in this study, we developed a HG-induced diabetic HK-2 cell model *in vitro*, and investigated the antifibrotic capacity of tFNAs, hoping to provide evidence for tFNAs as a potential alternative for future DKD treatment.

According to previous reports from our group, tFNAs were synthesized through the self-assembly of four designed single-stranded DNA (ssDNA) based on Watson-Crick base pairing principles [12,13]. The synthesis scheme is shown in Fig. 1A, and sequences of the four ssDNA strands are listed in Table S1 (Supporting information). The molecular weight of tFNAs was verified by polyacrylamide gel electrophoresis (PAGE) and high-performance capillary electrophoresis (HPCE). Results in Figs. 1B and C showed that the molecular weight of tFNAs reached around 200 bp, and therefore tFNAs moved slower than the other four single strands and two half-assembled structures. Dynamic light scattering (DLS) further confirmed that the size (Fig. 1D) and zeta potential (Fig. 1E) of tFNAs are around 7.689 nm and −8.97 mV, respectively. Transmission electron microscopy (TEM) and atomic force microscopy (AFM) were employed to observe the morphologies of tFNAs, illustrating the triangle-shaped nanostructure of tFNAs (Figs. 1F and G).

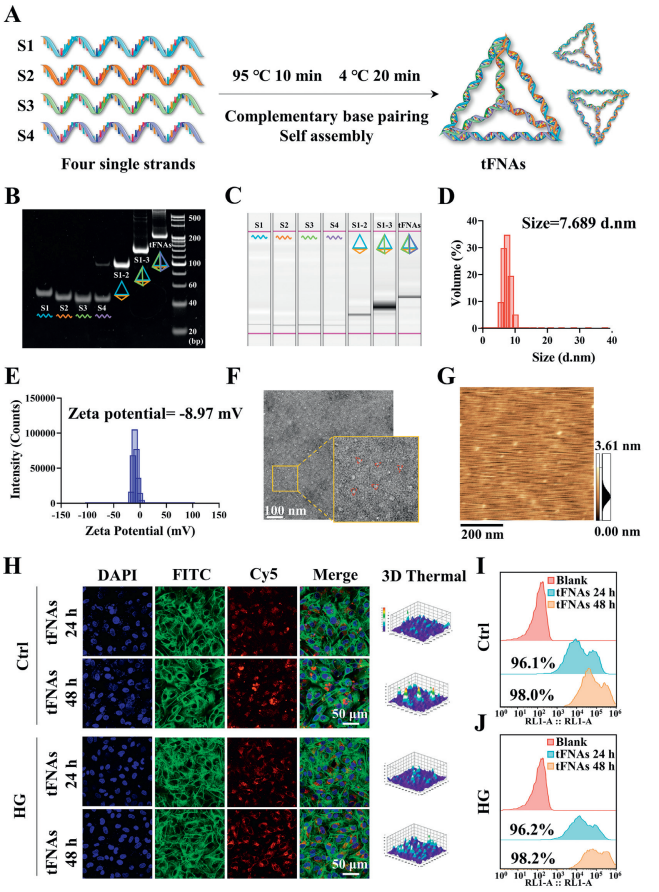

Fig. 1. Fabrication and characterization of tFNAs. (A) Schematic illustration of the synthesis process of tFNAs. (B) PAGE was applied to verify the successful synthesis of tFNAs. (C) HPCE was applied to evaluate the molecular weight of S1–2, S1–3, and tFNAs. (D) DLS was used to detect the hydrated size of tFNAs. (E) Zeta potential distribution of tFNAs. (F) TEM was employed to characterize the morphologies of tFNAs. Scale bar: 100 nm. (G) AFM images of tFNAs. Scale bar: 200 nm. (H) Fluorescence images for cellular uptake of Cy5-tFNAs in the Ctrl and HG groups. Cytoskeleton: green; Cy5: red; 4′,6-diamidino-2-phenylindole (DAPI): blue. Scale bar: 50 μm. (I, J) Flow cytometric results for cellular uptake of Cy5-tFNAs in the Ctrl and HG groups.

The aforementioned results suggested our successful fabrication of tFNAs for subsequent studies.

Since effective internalization of tFNAs is the prerequisite for conducting intracellular biological effects, exploring the HK-2 cellular uptake characteristic of tFNAs in both normal and HG states is important. Confocal fluorescence images observed the relationship between Cy5-tFNAs and HK-2 cell structures *in situ*. As is shown in Fig. 1H, there were similar endocytosis trends between the Ctrl and HG groups. First, after 24 h incubation, many Cy5-tFNAs successfully entered and were distributed in the cytoplasm of HK-2 cells. As time passed, the intracellular Cy5 fluorescence intensity in the two states both became even stronger after 48 h, indicating the stable and long-lasting internalization of tFNAs. Previous studies have found that tFNAs can be autonomously and efficiently internalized without other delivery assistance, possibly *via* the caveolin-dependent pathway and macropinocytosis-related protein sorting nexin 5 (SNX5) [32-34]. Additionally, flow cytometry was applied to quantify the cellular uptake proportion. Consistent with fluorescence detection results, uptake of tFNAs in normal (Ctrl) and diabetic (HG) HK-2 cells both achieved a relatively high level in 24 h and slightly increased until 48 h. The internalization in the Ctrl group increased from 96.1% to 98.0%, while that of the HG group was 96.2% and 98.2% (Figs. 1I and J). These results proved

that tFNAs can successfully penetrate cell membranes and be well-compatible with HK-2 cells. Moreover, we performed a cell counting kit-8 (CCK-8) assay to determine an appropriate concentration of tFNAs for further therapy. As illustrated in Fig. S1 (Supporting information), no obvious negative adverse effects on cell viability were observed among the five concentration gradients, and 250 nmol/L exhibited a slight advantage over other concentrations. Referring to previous studies, 250 nmol/L tFNAs generally exhibited the optimal cytoprotective effects [35,36], and therefore were finally selected for subsequent studies.

HG concentrations can directly induce excessive production of ROS and activate many pro-inflammatory signaling pathways, exerting a synergistic role in exacerbating DKD renal fibrosis. On the one hand, HG-induced mitochondria dysfunction leads to ROS over-accumulation, which subsequently participates in the nonenzymatic glycation reactions of reducing sugars like glucose and promotes advanced glycation end products (AGE) formation [37,38]. On the other hand, HG-derived AGEs as a potent pro-inflammatory factor could activate various inflammatory signaling pathways, aggravating intracellular oxidative stress in return [7]. Consequently, blocking the vicious circle *via* ROS-scavenging can be a feasible access to prevent the further development of diabetic diseases [39]. Several previous studies have reported the antioxidative properties of tFNAs in diabetic disease models, including glucosamine (GlcN)-induced insulin resistance (IR) [40], AGEs-induced angiogenesis deficiency [25,41,42] and diabetic osteoporosis [43,44]. However, the ROS-scavenging ability of simple tFNAs in HG renal tubular epithelial cells has not been investigated yet. Hence, flow cytometry and fluorescence assays were performed *via* the 2′,7′-dichlorodihydrofluorescein diacetate (DCFH-DA) fluorescent probe to compare the intracellular ROS changes among normal (Ctrl), diabetic (HG), and prevented (HG + tFNAs) HK-2 cells. ROS can oxidize nonfluorescent DCFH and become fluorescent DCF, and the fluorescence intensity is in direct proportion to the intracellular ROS concentrations. As the flow cytometrical analysis showed in Fig. 2A, the intracellular ROS was kept at a moderate level in normal states to guarantee necessary signal transduction and metabolic activities. However, stimulated by HG, ROS production in the HG group was upregulated for about 13%, inducing oxidative stress. In contrast, incubated with 250 nmol/L tFNAs for 48 h prevention, the ROS level in the HG group was effectively downregulated for around 7%, becoming closer to the normal state. The same inhibitory effect was also observed in confocal fluorescence images, confirming the antioxidative advantage of tFNAs (Fig. 2B).

Accumulating evidence indicates that the nuclear factor erythroid 2-related factor 2 (Nrf2) is an essential target of the antioxidative activities of tFNAs [45,46]. Nrf2 is a pro-survival transcription factor that extensively participates in antioxidation, anti-inflammation, and anti-apoptosis processes, tightly interrelating with the serine and threonine kinase (Akt) and heme oxygenase-1 (HO-1) [47,48]. To further figure out the underlying antioxidative mechanism of tFNAs, we established a chronic diabetic model *in vitro* and evaluated the protein and mRNA expression level of Akt/Nrf2/HO-1 signaling after coculture for 48–72 h. The activation degree of Akt signaling is assessed by the ratios of phosphorylated Akt (p-Akt) and total Akt. Western blot (WB) results and semi-quantification analysis showed that compared to normal cells, Akt phosphorylation proportion in the HG group was evidently decreased to 0.56-fold, indicating the impairment of protective defense. In contrast, pre-treatment by tFNAs effectively activated Akt signaling, increasing the protein expression of p-Akt up to 0.73-fold. In response to HG-induced oxidative stress, HK-2 cells naturally upregulated the expression of Nrf2 and HO-1 protein, which was further enhanced by tFNAs. The relative protein expression of Nrf2 increased from 1.45-fold to 1.65-fold, while that of HO-1 increased from 1.39-fold to 1.53-fold (Figs. 2C and D). The results of the immunofluorescence staining analysis and quantitative polymerase chain reaction (qPCR) showed similar trends in Figs. 2E–H and Fig. S2 (Supporting information). Besides, it is also notable that the expression levels of Akt/Nrf2/HO-1 pathway in HG + tFNAs 48 h group were generally higher than that of HG + tFNAs 72 h group, which can be associated with two reasons. First, the qPCR results showed that the Kelch-like ECH-associated protein 1 (Keap1), an inhibitive factor of antioxidative Nrf2, was downregulated upon HG stimulation, and the degree was attenuated after 72 h, therefore decreasing the expression of Nrf2/HO-1. Moreover, with the treatment of tFNAs and disease recovery, downstream accumulated high concentrations of HO-1 would possibly inhibit the continuous activation of upstream p-Akt and Nrf2, thus maintaining intracellular homeostasis *via* a negative feedback mechanism.

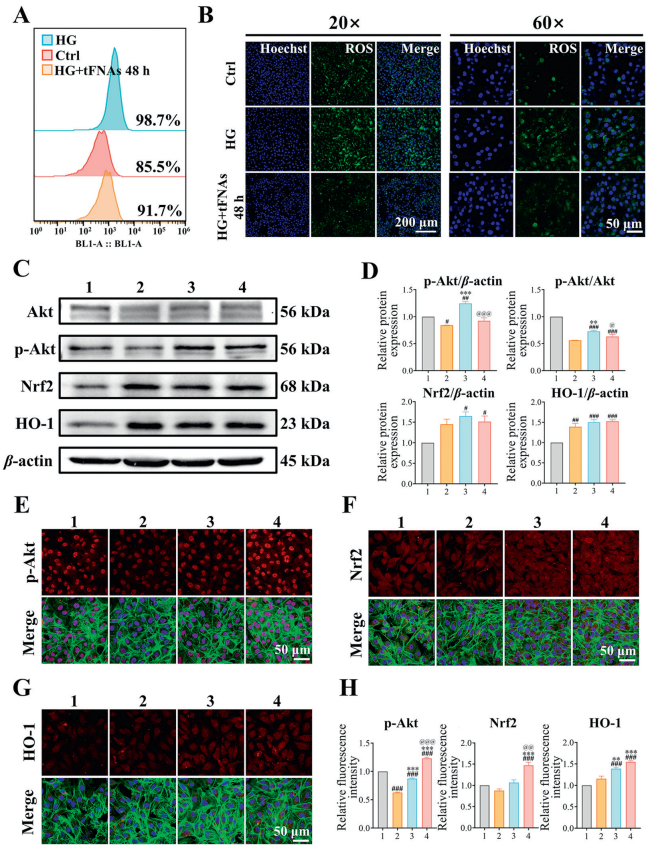

Fig. 2. tFNAs suppressed HG-induced oxidative stress *via* ROS-scavenging and Akt/Nrf2/HO-1 pathway. (A) Flow cytometric results for intracellular ROS fluorescence detection. (B) Fluorescence images for intracellular ROS fluorescence detection. ROS: green; Hoechst: blue. Scale bar: 200 μm (20×) and 50 μm (60×). (C) WB was used to evaluate the expression of Akt, p-Akt, Nrf2, and HO-1 proteins. (D) Statistical analysis of relative protein expression of antioxidative pathway. (E–H) Immunofluorescence staining and quantitative analysis of p-Akt, Nrf2, HO-1 protein. Cytoskeleton: green; p-Akt/Nrf2/HO-1: red; DAPI: blue. Scale bar: 50 μm. Group settings: 1-Ctrl, 2-HG, 3-HG + tFNAs 48 h, 4-HG + tFNAs 72 h. Data are presented as mean ± standard deviation (SD) ($n = 3$). $^{\#}P < 0.05$, $^{\#\#}P < 0.01$, $^{\#\#\#}P < 0.001$ *vs.* the control group; $^{*}P < 0.05$, $^{**}P < 0.01$, $^{***}P < 0.001$ *vs.* the HG-treated group; $^{@}P < 0.05$, $^{@@}P < 0.01$, $^{@@@}P < 0.001$ *vs.* the HG + tFNAs 48 h group.

HG-induced oxidative stress is a pivotal factor mediating cellular inflammatory reaction, gradually developing into a chronic state and further stimulating fibrogenic translation. Extensive studies have revealed that HG can directly and indirectly increase the pro-inflammatory activities of nuclear factor kappa-B (NF-κB) and mitogen-activated protein kinase (MAPK) pathway through complicated signaling networks, ultimately resulting in uncontrolled inflammation mediated by TNF-α, IL-1β and IL-6 [49-51]. However,

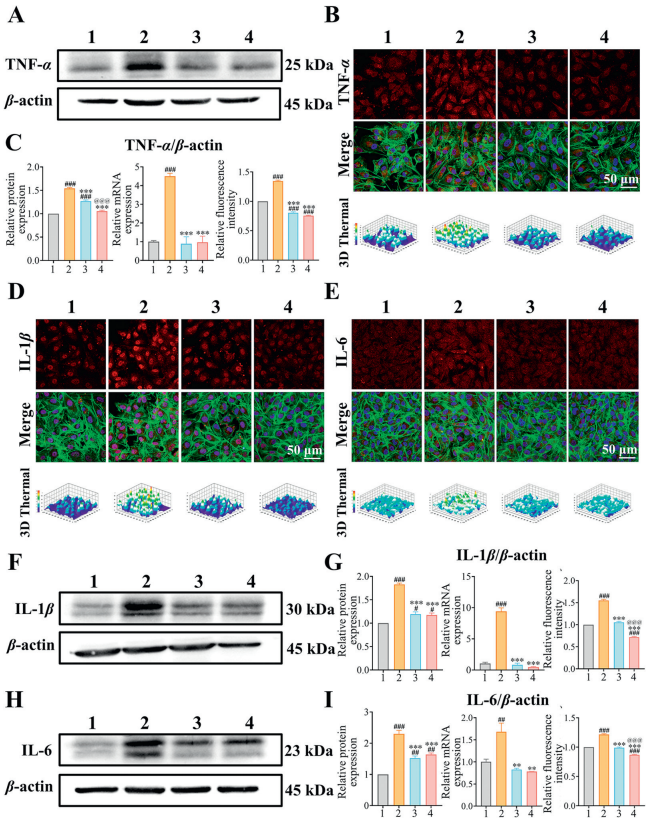

Fig. 3. tFNAs inhibited the expression of pro-inflammatory factors induced by HG. (A) WB results of TNF-α protein. (B) Immunofluorescence staining and 3D-thermal images of TNF-α. Cytoskeleton: green; TNF-α: red; DAPI: blue. Scale bar: 50 μm. (C) Statistical analysis of relative protein, mRNA, and fluorescence expression of TNF-α. (D, E) Immunofluorescence staining and 3D-thermal images of IL-1β and IL-6. Cytoskeleton: green; IL-1β/IL-6: red; DAPI: blue. Scale bar: 50 μm. (F) WB results of IL-1β protein. (G) Statistical analysis of relative protein, mRNA, and fluorescence expression of IL-1β. (H) WB results of IL-6 protein. (I) Statistical analysis of relative protein, mRNA, and fluorescence expression of IL-6. Group settings: 1-Ctrl, 2-HG, 3-HG + tFNAs 48 h, 4-HG + tFNAs 72 h. Data are presented as mean ± SD ($n = 3$). $^{\#}P < 0.05$, $^{\#\#}P < 0.01$, $^{\#\#\#}P < 0.001$ *vs.* the control group; $^{*}P < 0.05$, $^{**}P < 0.01$, $^{***}P < 0.001$ *vs.* the HG-treated group; $^{@}P < 0.05$, $^{@@}P < 0.01$, $^{@@@}P < 0.001$ *vs.* the HG + tFNAs 48 h group.

previous studies have well-demonstrated that tFNAs are innately endowed with the ability to regulate inflammatory pathways such as phosphatidylinositide 3-kinases (PI3K)/Akt [41,52], NF-κB [53], MAPK [19], becoming a promising anti-inflammatory strategy in HG conditions. Herein, we monitored the expression level of three dominant pro-inflammatory molecules in DKD, including TNF-α, IL-1β, and IL-6, aiming to explore the chronic anti-inflammatory capacity of tFNAs. As the WB and immunofluorescence staining results indicated in Figs. 3A and B, the relative protein production of TNF-α was significantly increased after 72 h HG coculture, reaching approximately 1.54-fold (Fig. 3C). However, with the prevention of tFNAs, not only the TNF-α protein concentrations were effectively decreased to 1.27-fold after 48 h and 1.05-fold after 72 h, the mRNA levels also declined from 4.75-fold to 1.58-fold and 1.34-fold (Fig. 3C). Likewise, generation of IL-1β and IL-6 was also detected, and both of them were observed with apparent suppression in fluorescence intensity due to the anti-inflammatory property of tFNAs (Figs. 3D and E). After up to 72 h pre-incubation, tFNAs inhibited nearly 36% expression of IL-1β protein and 94% mRNA (Figs. 3F and G), while that of IL-6 respectively account for 29% and 62% (Figs. 3H and I). Based on the tight association between the renal tubular epithelial cells fibrogenic translation and aforementioned molecular mechanisms [54], it can be concluded from Fig. 3 that tFNAs can well satisfy the anti-inflammation requirement for DKD prevention, and the effect can continue until at least 72 h *in vitro*.

Chronic inflammation constantly stimulates the profibrotic process of renal tubular epithelial cells, resulting in excessive extracellular matrix (ECM) deposition and renal tubulointerstitial fibrosis (TIF) [55]. The primary source of increased ECM is ascribed to myofibroblast, a pathologically differentiated cell phenotype characterized by elevated α-smooth muscle actin (α-SMA) expression and collagen I secretion [56]. Many researchers have reported the diverse and complicated constitution of the myofibroblast pool, in which tubular epithelial cells are considered a significant contributor [57]. Under HG circumstances, renal tubular epithelial cells can be injured by multiple factors, such as aforementioned oxidative stress and chronic inflammation, thus involved in the EMT process and translating into myofibroblasts [58-60]. Although the original significance of EMT lies in self-defense and recovery promotion, sustaining activation of EMT eventually reverses the outcome into harmful and even irreversible renal fibrosis [57,61].

Consequently, to evaluate the extent of HG-mediated profibrosis and tFNAs-mediated antifibrosis, we detected and quantified the expression levels of collagen I and α-SMA in diabetic and tFNAs-prevented HK-2 cells. Based on WB results presented in Figs. 4A and B, incubation with HG for 72 h obviously upregulated the protein expression of collagen I and α-SMA, which indicated that HG successfully induced the EMT process and facilitated the fibrogenesis activity of HK-2 cells. In contrast, tFNAs successfully downregulated these two fibrogenic indicators to a nearly normal state, and the efficacy increased from 48 h to 72 h. Immunofluorescence staining and semi-quantification analysis illustrated in Figs. 4C and D showed that pre-incubation with HG HK-2 cells with 250 nmol/L tFNAs significantly decreased the relative fluorescence intensity of collagen I from 1.30-fold to around 0.74-fold, with that of α-SMA declined from 1.64-fold to 1.10-fold in 48 h and 0.76-fold in 72 h, which is consistent with the WB results. Similar results were also obtained by qPCR statistical analysis (Fig. 4D), confirming the efficient EMT and fibrogenesis alleviation by tFNAs in pathological HG circumstances.

In previous studies, tFNAs also exhibited both natural and functionally enhanced antifibrotic advantages. For instance, simple tFNAs can already achieve scarless cutaneous wound healing *via* the Akt pathway [23,41], in which healing peptides can further strengthen to promote angiogenesis *via* the ERK1/2 pathway [25]. Multiple pathways are involved in fibrotic development, including TGF-β, NF-κB, NOTCH, and the dominant Wnt/β-catenin pathway in the diabetic EMT process [62]. During EMT progression, renal tubular epithelial cells as the primary contributor of Wnt factor upon various stimulations will upregulate the β-catenin concentrations in the cytoplasm. Over-activated β-catenin subsequently translocates into the nucleus and combines with lymphoid enhancer factor-dependent gene (Lef1), forming a functional complex to trigger downstream gene expression such as α-SMA, and cyclin D1 [61,63]. α-SMA, the biomarker of myofibroblasts as we mentioned before, characterizes the EMT progression. While cyclin D1 participates in the premature senescence of renal tubular cells, whose excessive increase results in chronic tubular injury and fibrosis [64]. In our study, in order to further elucidate the underlying molecular mechanism of EMT inhibition and fibrogenesis attenuation by tFNAs, we assessed the expression level of the Wnt/β-catenin pathway. According to the WB analysis results shown in Figs. 4E and F, 72 h incubation with HG obviously activated the Wnt/β-catenin pathway, with protein expression of β-catenin increased to 1.44-fold, Lef1 increased to 2.13-fold and cyclin D1 increased to 2.27-fold, compared to the control group. In contrast, pre-incubation with tFNAs helped to relieve Wnt-mediated EMT. After 48–72 h prevention, the expression level of β-catenin protein declined to around 1.10-fold, with Lef1 and cyclin D1 respectively

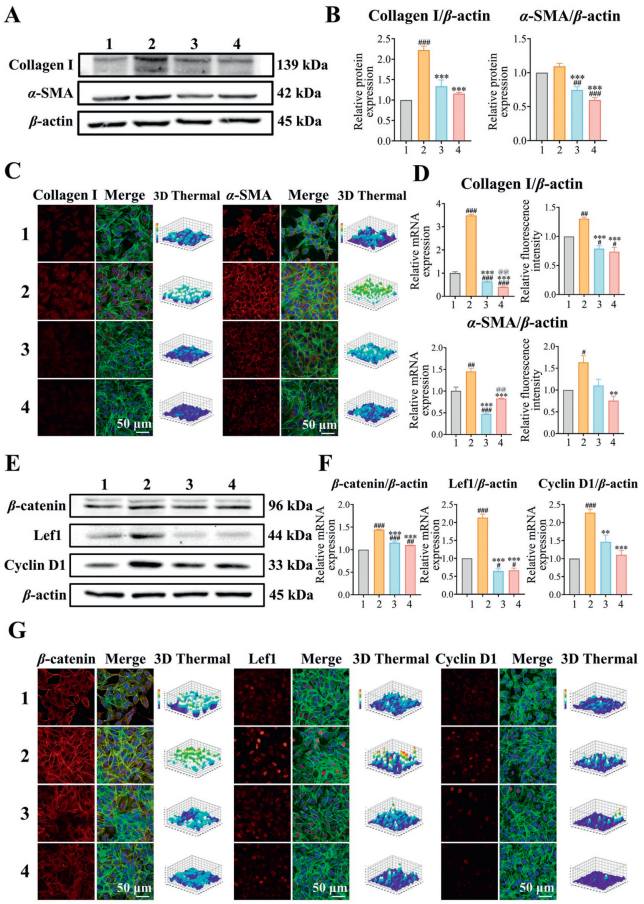

Fig. 4. tFNAs prevented the HG-mediated EMT process *via* down-regulating the Wnt/β-catenin pathway. (A, B) WB and semi-quantification results of collagen I and α-SMA protein expression. (C) Immunofluorescence staining and 3D-thermal images of collagen I and α-SMA. Cytoskeleton: green; Collagen I/α-SMA: red; DAPI: blue. Scale bar: 50 μm. (D) Statistical analysis of relative mRNA and fluorescence expression of Collagen I and α-SMA. (E, F) WB and semi-quantification results of the expression of β-catenin, Lef1, and cyclin D1 protein. (G) Immunofluorescence staining and 3D-thermal images of β-catenin, Lef1, and cyclin D1. Cytoskeleton: green; β-catenin/Lef1/cyclin D1: red; DAPI: blue. Scale bar: 50 μm. Group settings: 1-Ctrl, 2-HG, 3-HG + tFNAs 48 h, 4-HG + tFNAs 72 h. Data are presented as mean ± SD ($n = 3$). $^{\#}P < 0.05$, $^{\#\#}P < 0.01$, $^{\#\#\#}P < 0.001$ *vs.* the control group; $^{*}P < 0.05$, $^{**}P < 0.01$, $^{***}P < 0.001$ *vs.* the HG-treated group; $^{@}P < 0.05$, $^{@@}P < 0.01$, $^{@@@}P < 0.001$ *vs.* the HG + tFNAs 48 h group.

dropping to 0.65- and 1.47-fold. This trend was well matched with the immunofluorescence staining results demonstrated in Fig. 4G. In addition, we also examined the activation level of the Wnt/β-catenin pathway in terms of gene expression, and statistics suggested that tFNAs reduced nearly 38% β-catenin mRNA, 30% Lef1 mRNA and 29% cyclin D1 mRNA after 48 h prevention (Fig. S3 in Supporting information). However, all three indicators were picked up in the 72 h prevention group, possibly due to negative feedback inhibition from other regulatory factors [65]. As an essential regulator in embryonic development and adult tissue homeostasis, Wnt/β-catenin signaling extensively participates in various diseases and exhibits different mediation functions [66]. Several studies have explored regulations of tFNAs on the Wnt/β-catenin pathway, and the consequences vary based on different pathological backgrounds. In cutaneous wound healing and acute liver failure, tFNAs mainly contributed to promoting cell proliferation *via* reversing the downregulated Wnt signaling [42,67], while in osteoarthritis, tFNAs helped chondrocytes survival *via* Wnt inhibition [21]. In our study, unbalanced activation of the Wnt/β-catenin pathway in HG-induced tubular epithelial cells EMT was successfully rectified by tFNAs, providing more evidence for DKD management through targeting the Wnt/β-catenin signaling pathway.

In conclusion, under long-term HG circumstances, renal tubular epithelial cells continuously underwent oxidative stress, inflammation, and EMT process, which jointly result in pro-fibrogenic phenotype translation and mass production of collagen, ultimately manifesting as progressing renal fibrosis. However, the advent of novel tFNA nanostructures brings the stable, biocompatible, and tailorable antifibrotic strategy into reality. Extensive studies have confirmed that self-assembled tFNAs can be not only facilitated to penetrate the cell membrane and regulate cell behavior but also highly open to composite functionalized systems with miRNA, peptide, aptamers and so on, realizing targeted drug delivery and responsive drug release [68-70]. In this study, taking advantage of the excellent biological properties of tFNAs, we successfully achieved antioxidation and anti-inflammation therapy through ROS-scavenging and modulations on the Akt/Nrf2/HO-1 pathway. Furthermore, tFNAs effectively prevented the fibrogenesis process in diabetic HK-2 cells by inhibiting the activation of the EMT-related Wnt/β-catenin signaling pathway. Hitherto, pharmacotherapy of renal fibrosis mainly relies on RAAS blockers and some Chinese traditional medicine, but the effect remains unsatisfactory, partly due to short biological half-life and poor water solubility. Our primary exploration of the naturally antifibrotic potential of tFNAs provides a wide field for further development of functionalized tFNAs-derived drug delivery platforms, which could make up the drawbacks mentioned above to the maximum and bring more secure, efficient as well as controllable strategy for DKD management.

Declaration of competing interest

The authors declare that they have no known competing financial interests or personal relationships that could have appeared to influence the work reported in this paper.

CRediT authorship contribution statement

Yujie Zhu: Writing – original draft, Visualization, Investigation, Formal analysis, Data curation, Conceptualization. **Ruijianghan Shi:** Writing – review & editing, Investigation, Data curation, Conceptualization. **Weitong Lu:** Methodology, Formal analysis, Data curation, Conceptualization. **Yang Chen:** Writing – review & editing, Supervision, Project administration. **Yunfeng Lin:** Writing – review & editing, Supervision, Project administration, Funding acquisition. **Sirong Shi:** Writing – review & editing, Supervision, Project administration, Methodology, Funding acquisition.

Acknowledgments

This study was supported by the National Natural Science Foundation of China (No. 82101077), Sichuan Science and Technology Program (No. 2023NSFSC1516), Postdoctoral Science Foundation of China (Nos. 2021M692271, 2023T160455), West China School/Hospital of Stomatology Sichuan University, No. RCDWJS2023–5, Fundamental Research Funds for the Central Universities, and Research and Develop Program, West China Hospital of Stomatology Sichuan University. The authors would like to thank Liying Hao (State Key Laboratory of Oral Diseases, National Clinical Research Center for Oral Diseases, West China Hospital of Stomatology, Sichuan University) for her help in characterizing AFM. Graphical abstract image is created with BioRender.com, with permission.

Supplementary materials

Supplementary material associated with this article can be found, in the online version, at doi:10.1016/j.cclet.2024.110140.

References

[1] Q. Hu, L. Jiang, Q. Yan, et al., Pharmacol. Ther. 241 (2023) 108314.
[2] P.H. Hung, Y.C. Hsu, T.H. Chen, C.L. Lin, Int. J. Mol. Sci. 22 (2021) 11857.
[3] G. Tang, S. Li, C. Zhang, et al., Acta Pharm. Sin. B 11 (2021) 2749–2767.
[4] Y. Zheng, S.H. Ley, F.B. Hu, Nat. Rev. Endocrinol. 14 (2017) 88–98.
[5] S.C.W. Tang, W.H. Yiu, Nat. Rev. Nephrol. 16 (2020) 206–222.
[6] R. Qi, C. Yang, Cell Death Dis. 9 (2018) 1126.
[7] Q. Hu, Y. Chen, X. Deng, et al., Biomed. Pharmacother. 159 (2023) 114252.
[8] R. Huang, L. He, L. Jin, et al., Chin. Chem. Lett. 34 (2023) 107926.
[9] T. Zhang, T. Tian, Y. Lin, Adv. Mater. 34 (2022) 2107820.
[10] Z. Guo, B. Jin, Y. Fang, et al., Chin. Chem. Lett. 33 (2022) 4208–4212.
[11] R.P. Goodman, R.M. Berry, A.J. Turberfield, Chem. Commun. (2004) 1372–1373.
[12] T. Zhang, T. Tian, R. Zhou, et al., Nat. Protoc. 15 (2020) 2728–2757.
[13] Y. Lin, Q. Li, L. Wang, et al., Int. J. Oral Sci. 14 (2022) 51.
[14] Y. Guo, J. Tang, C. Yao, D. Yang, WIREs Nanomed. Nanobiotechnol. 14 (2021) e1753.
[15] W. Chen, B.C. Yung, Z. Qian, X. Chen, Adv. Drug Deliv. Rev. 127 (2018) 20–34.
[16] L. Chen, W. Hong, W. Ren, et al., Signal Transduct. Target. Ther. 6 (2021) 351.
[17] L. Chen, J. Zhang, Z. Lin, et al., Acta Pharm. Sin. B 12 (2022) 76–91.
[18] L. Wang, M.L. Javier, C. Luo, et al., Chin. Chem. Lett. 35 (2024) 109591.
[19] M. Zhou, S. Gao, X. Zhang, et al., Bioact. Mater. 6 (2021) 1676–1688.
[20] Z. Guo, B. Jin, Y. Fang, et al., Chin. Chem. Lett. 35 (2024) 108528.
[21] S. Shi, T. Tian, Y. Li, et al., ACS Appl. Mater. Interfaces 12 (2020) 56782–56791.
[22] H. Wang, J. Gong, W. Chen, et al., Nano Today 56 (2024) 102252.
[23] J. Zhu, M. Zhang, Y. Gao, et al., Signal Transduct. Target. Ther. 5 (2020) 120.
[24] C. Cai, T. Wang, X. Han, et al., Chin. Chem. Lett. 33 (2022) 1963–1969.
[25] S. Lin, Q. Zhang, S. Li, et al., Cell Prolif. 55 (2022) e13279.
[26] T. Tian, C. Zhao, S. Li, et al., ACS Appl. Mater. Interfaces 15 (2023) 10492–10505.
[27] L. Yao, J. Li, X. Qin, et al., ACS Mater. Lett. 5 (2023) 1153–1163.
[28] R. Yan, W. Cui, W. Ma, et al., ACS Nano 17 (2023) 8767–8781.
[29] Y.H. Zhang, Y.Q. Zhang, C.C. Guo, et al., Acta Pharmacol. Sin. 41 (2019) 561–571.
[30] Q. Lu, L. Yang, J.-J. Xiao, et al., Free Radic. Biol. Med. 195 (2023) 89–102.
[31] D. Yuan, H. Li, W. Dai, et al., Biochim. Biophys. Acta Mol. Basis Dis. 1870 (2024) 167022.
[32] L. Liang, J. Li, Q. Li, et al., Angew. Chem. Int. Ed. 53 (2014) 7745–7750.
[33] C. Mao, W. Pan, X. Shao, et al., ACS Appl. Mater. Interfaces 11 (2018) 1942–1950.
[34] T. Tian, C. Zhang, J. Li, et al., Small 17 (2021) e2100837.
[35] Q. Zhang, S. Lin, S. Shi, et al., ACS Appl. Mater. Interfaces 10 (2018) 3421–3430.
[36] M. Zhou, T. Zhang, X. Zhang, et al., ACS Appl. Mater. Interfaces 14 (2022) 37478–37492.
[37] K. Nowotny, T. Jung, A. Höhn, D. Weber, T. Grune, Biomolecules 5 (2015) 194–222.
[38] A.G. Miranda-Díaz, L. Pazarín-Villaseñor, F.G. Yanowsky-Escatell, J. Andrade-Sierra, J. Diabetes Res. 2016 (2016) 7047238.
[39] S. Feng, Y. Qu, B. Chu, et al., Kidney Int. 102 (2022) 1057–1072.
[40] Y. Li, Y. Tang, S. Shi, et al., ACS Appl. Mater. Interfaces 13 (2021) 40354–40364.
[41] S. Lin, Q. Zhang, S. Li, et al., ACS Appl. Mater. Interfaces 12 (2020) 11397–11408.
[42] Z. Wang, H. Lu, T. Tang, et al., Cell Prolif. 55 (2022) e13316.
[43] L. Bai, M. Feng, Q. Zhang, et al., Adv. Funct. Mater. 34 (2024) 2314789.
[44] Y. Li, J. Li, Y. Chang, Y. Lin, L. Sui, Chin. Chem. Lett. 35 (2024) 109414.
[45] M. Zhang, X. Zhang, T. Tian, et al., Bioact. Mater. 8 (2022) 368–380.
[46] Y. Li, Z. Cai, W. Ma, et al., Bone Res. 12 (2024) 14.
[47] A. Cuadrado, A.I. Rojo, G. Wells, et al., Nat. Rev. Drug Discov. 18 (2019) 295–317.
[48] A. Loboda, M. Damulewicz, E. Pyza, A. Jozkowicz, J. Dulak, Cell. Mol. Life Sci. 73 (2016) 3221–3247.
[49] F. Xu, H. Jiang, X. Li, et al., Adv. Sci. 11 (2023) 2306704.
[50] G. Ke, X. Chen, R. Liao, et al., Kidney Int. 100 (2021) 377–390.
[51] Y. Zhong, K. Lee, Y. Deng, et al., Nat. Commun. 10 (2019) 4523.
[52] X. Zhou, Y. Lai, X. Xu, et al., Cell Prolif. 56 (2023) e13407.
[53] X. Chen, J. He, Y. Xie, et al., Cell Prolif. 56 (2023) e13424.
[54] W.J. Huang, W.J. Liu, Y.H. Xiao, et al., Biomed. Pharmacother. 121 (2020) 109599.
[55] M. Khokhar, D. Roy, A. Modi, et al., Crit. Rev. Clin. Lab. Sci. 57 (2020) 470–483.
[56] M. Edeling, G. Ragi, S. Huang, H. Pavenstädt, K. Susztak, Nat. Rev. Nephrol. 12 (2016) 426–439.
[57] Y. Ovadya, V. Krizhanovsky, Nat. Med. 21 (2015) 975–977.
[58] L. Du, Y. Chen, J. Shi, et al., Metabolism 144 (2023) 155376.
[59] L. Zhou, D.Y. Xu, W.G. Sha, et al., J. Transl. Med. 13 (2015) 352.
[60] J. Zhou, X. Peng, Y. Ru, J. Xu, Inflammation 45 (2022) 1911–1923.
[61] S.J. Schunk, J. Floege, D. Fliser, T. Speer, Nat. Rev. Nephrol. 17 (2020) 172–184.
[62] T.A. Wynn, T.R. Ramalingam, Nat. Med. 18 (2012) 1028–1040.
[63] S. Zhou, Q. Wu, X. Lin, et al., Kidney Int. 99 (2021) 364–381.
[64] C. Jia, C. KeHong, X. Fei, et al., Kidney Int. 98 (2020) 645–662.
[65] A. Niida, T. Hiroko, M. Kasai, et al., Oncogene 23 (2004) 8520–8526.
[66] J. Liu, Q. Xiao, J. Xiao, et al., Signal Transduct. Target. Ther. 7 (2022) 3.
[67] Y. Chen, S. Shi, B. Li, et al., ACS Appl. Mater. Interfaces 14 (2022) 13136–13146.
[68] T. Tian, D. Xiao, T. Zhang, et al., Adv. Funct. Mater. 31 (2020) 2007342.
[69] L. Zhang, L. Xu, Y. Wang, et al., Chin. Chem. Lett. 33 (2022) 4089–4095.
[70] Y. Ge, Q. Wang, Y. Yao, et al., Adv. Sci. 11 (2024) 2308701.